Computational and Theoretical Chemistry 1193 (2021) 113047

Contents lists available at ScienceDirect

Computational and Theoretical Chemistry

journal homepage: www.elsevier.com/locate/comptc

The adsorption of bromochlorodifluoromethane on pristine, Al, Ga, P, and As-doped boron nitride nanotubes: A study involving PBC-DFT, NBO analysis, and QTAIM

Mohsen Doust Mohammadi [a], Hewa Y. Abdullah [b,*]

[a] School of Chemistry, College of Science, University of Tehran, Tehran 14176, Iran
[b] Physics Education Department, Faculty of Education, Tishk International University, 44001 Erbil, Iraq

ARTICLE INFO

Keywords:
Bromochlorodifluoromethane
Halon 1211 BCF
Boron nitride
Density functional theory
Halon 1211
Natural bond orbital

ABSTRACT

Nanostructures such as nanotubes and nanosheets are widely used in the medical industry for drug delivery, prevention, and treatment. These nanostructures are used as sensors or carriers by adsorbing functional groups. In this study, the adsorption rates of the bromochlorodifluoromethane ($CBrClF_2$) molecule, which is used as an effective gaseous fire suppression agent, onto the outer surfaces of pristine, Al, Ga, P, and As-doped boron nitride nanotubes are investigated. A periodic boundary condition density functional theory method using both Perdew, Burke, and Ernzerhof exchange–correlation (PBEPBE) and B3LYP-D3 functionals together with the 6-311G (d) basis set were used. Subsequently, the B3LYP, CAM-B3LYP, ωB97XD, and M06-2X functionals with the 6-311G (d) basis set were used to consider the single-point energies. Natural bond orbital analysis and the quantum theory of atoms in molecule were considered using the PBEPBE/6-311G (d) method, and the results were compatible with the expected electronic properties, namely the Wiberg bond index, natural charge, natural electron configuration, donor–acceptor natural bond orbital interactions, and second-order perturbation energies. All the calculations and analyses denoted that the adsorption of the $CBrClF_2$ molecule onto the surfaces of pristine boron nitride nanotubes occurred due to physical adsorption and van der Waals interactions. Among the doped nanotubes, the Al nanotube exhibited the highest adsorption energy compared to the other doped nanotubes.

1. Introduction

Nanotubes are structurally divided into carbon and non-carbon nanotubes. Carbon nanotubes (CNTs) were first discovered independently by Iijima and Ichihashi in 1991 in soot from carbon discharge in a neon-containing medium [1]. CNTs can pass through cell walls because of their needle shape [2]. Various studies have shown that single-walled nanotubes are potentially very good agents for the delivery of anticancer drugs [3,4]. However, the toxicity of CNTs to tissues is still being studied [5]. Since the discovery of CNTs, many efforts have been made to discover non-CNTs due to the dependence of the properties of CNTs on the nanotube diameter and chiral features. Thereafter, boron nitride nanotubes (BNNTs) were first synthesized in 1995 [6]. These nanotubes, similar to their carbon counterparts, have excellent mechanical properties due to the strong sp^3 bonds in the nanotube walls [7,8].

BNNTs are characterized by remarkable mechanical and electrical properties, such as a wide band gap (3.5–5.5 eV) [9], good piezoelectric properties, high thermal and chemical stability [10], and high oxidation resistance [11,12]. Their unique mechanical properties and high thermal conductivity [13] are invaluable for diagnostic and therapeutic approaches to diseases as well as sensor-based applications. BNNTs are hydrophobic and insoluble in water, and their resistance to oxidation makes them useful as drug carriers [14]. In addition, BNNTs are non-toxic to cells. They do not damage the DNA [15]. Ciofani et al. tested the non-toxicity of BNNTs [16,17]. Their results showed that the chemical neutrality and structural stability of these nanotubes is attributable to their biocompatibility [18].

Following the discovery of BNNTs in 1994 by Rubio et al. [19] and their synthesis by Chopra et al. in 1995 [6,20], Deca et al. studied the interactions between the (10, 0) and (10, 5) nanotubes with the drug molecule isoniazid (INH) [21]. They showed that the binding energy of INH to BNNT (5, 5) was slightly higher than that of BNNT (10, 0).

* Corresponding author.
E-mail address: hewayaseen@gmail.com (H.Y. Abdullah).

https://doi.org/10.1016/j.comptc.2020.113047
Received 11 July 2020; Received in revised form 13 September 2020; Accepted 28 September 2020
Available online 6 October 2020

Mukhopadhyay et al. studied the adsorption of tryptophan (a non-polar amino acid), sparic acid, and arginine (a polar amino acid) on BNNTs, and reported a strong bonding energy for the adsorption of the polar amino acid on the BNNT surface [22]. Peyghan et al. investigated the adsorption and electrical structure of the BNNT (6, 0) imidazole molecule in the gaseous and soluble phases. They found that imidazole adsorption had no significant effect on the electrical structure of the BNNT [23]. Yang et al. studied the interaction between BNNTs with biological molecules using density-functional theory (DFT) calculations [24]. Anota et al. investigated the interaction between BNNT and metformin using DFT [25]. Recently, the interaction between the uracil molecule and BNNT (n, 0) was investigated by Mirzai et al. [26]. Given the widespread use of BNNTs, many theoretical investigations have been conducted on the adsorption of different molecules onto the surface of various nanostructures, such as aluminum nitride and silicon carbide [27–34].

Bromochlorodifluoromethane (BCF), also known as halon 1211, halon 1211 BCF, or freon 12B1, has many applications in industries as well as daily life. BCF is a proficient fire extinguishing agent and exhibits lower toxicity compared to carbon tetrachloride [35,36]. The BCF is classified as a chlorofluorocarbon; therefore, its ozone depletion potential is high. Care should be taken when using this substance, and currently, the production of BCF is limited in most countries, but it continues to be recycled. Similar investigations have been performed to detect Ozone-depleting substances. For example Scaranto et al. theoretically studied the CH_2BrF adsorption on TiO_2 surface [37], Mohammadi et al. provided DFT modelling for adsorption of CH_3Br using different nanotubes [28], Esrafili et al. performed a study on N_2O [38], Gholizadeh et al investigated the adsorption of CO on Si-and Se-doped graphenes [39]. Other pollutants are also studied like Hydrochlorofluorocarbons [40], NO [41], CH_2F_2 [42], NO2 and NO3 [43]. Accordingly, it is important to study the feasibility of the adsorption of BCF by using the nano-material surface.

This article discusses the design of such a sensor. This study investigated the interactions of BCF with BNNT and BN nanotubes doped with Al, Ga, P, and As. The structure of BN was optimized using Gaussian software to study the chemical stability and conductivity characteristics, following which the element doping process was investigated. Different structures need to be optimized using appropriate computational methods. The computation method should be highly sensitive to precisely determine the energies of the molecular orbitals and allow an in-depth understanding of the conductivity and probability of physical and chemical adsorption. For this purpose, the Perdew, Burke, and Ernzerhof exchange–correlation (PBEPBE) as well as B3LYP-D3 functionals and 6-311G (d) basis set were used in this research for the computations. The B3LYP, CAM-B3LYP, ωB97XD, and M06-2X functionals with the 6-311G (d) basis set were also used to calculate the single-point energies. The natural bond orbital (NBO) and quantum theory of atoms in molecule (QTAIM) were implemented with the PBEPBE/6-311G (d) method, and the results were used to obtain various physical parameters.

2. Computational details

The periodic boundary condition DFT (PBC-DFT) calculations at both PBEPBE [44] and B3LYP-D3 [45–47] functionals together with the 6-311G (d) Pople split-valence triple zeta basis set with polarization functions [48] were used for geometry optimization of all different positions of the BCF/nanotube complex structures. All the calculations, including geometry optimization, single-point energy calculations, and NBO analysis, were performed with the Gaussian 16 package [49,50]. It should be noted that NBO calculations were performed using the NBO v 3.1 software, which is embedded within Gaussian software. The Multiwfn program [51] was used to implement the QTAIM and density of state (DOS) analyses. The DOS diagrams were depicted using the GaussSum [52] package.

The adsorption energy (E_{ads}) of the BCF onto the surface of the pristine and doped nanotubes can be calculated as follows:

$$E_{ads} = E_{tube/BCF} - (E_{tube} + E_{BCF}) \tag{1}$$

where $E_{tube/BCF}$ represents the total energy of the complex structure. E_{tube} and E_{BCF} are the total energies of the pure nanotube and the pure BCF molecule, respectively.

The chemical electron potential (μ) describes the tendency of electrons to escape from a particular species at the ground state.

According to Parr [53] as well as Koopmans' [54] and Janak's approximations [55], the chemical potential is defined as

$$\mu = \left(\frac{\partial E}{\partial N}\right)_{\upsilon(\vec{r})} \cong \frac{(\varepsilon_{LUMO} + \varepsilon_{HOMO})}{2} \tag{2}$$

where ε_{HOMO} and ε_{LUMO} are the energies of the HOMO and the LUMO, respectively. N is the number of electrons, E is the total electronic energy of the system, and $\upsilon(r)$ is the external potential. The chemical hardness (η) and electrophilicity (ω) are expressed, respectively, as follows:

$$\eta = \left(\frac{\partial \mu}{\partial N}\right) = \frac{1}{2}\left(\frac{\partial^2 E}{\partial N^2}\right) \cong \frac{(\varepsilon_{LUMO} - \varepsilon_{HOMO})}{2} \tag{3}$$

$$\omega = \frac{\mu^2}{2\eta} \tag{4}$$

The Wiberg bond index (WBI) [56] identifies the bond order character and is denoted as follows:

$$WBI = \sum_k p_{jk}^2 = 2p_{jj} - p_{jk}^2 \tag{5}$$

where p_{jk} represents the density matrix elements, and p_{jj} is the charge density in the atomic orbital. Furthermore, the second-order perturbative estimate of donor–acceptor interactions as per the NBO analysis is defined by the second-order perturbation theory [57], as follows:

$$\Delta E_{i\to j}^2 = -2\frac{\left\langle \sigma_i \middle| \widehat{F} \middle| \sigma_j^* \right\rangle^2}{\varepsilon_{j^*} - \varepsilon_i} \tag{6}$$

where $\widehat{F}$ is the effective orbital Hamiltonian, $\varepsilon_i = \left\langle \sigma_i \middle| \widehat{F} \middle| \sigma_i \right\rangle$, and $\varepsilon_{j^*} = \left\langle \sigma_j^* \middle| \widehat{F} \middle| \sigma_j^* \right\rangle$.

3. Results and discussion

3.1. Structural analysis

To optimize the structure of pristine armchair (5, 5) single-walled BNNTs using periodic boundary conditions, we first considered a base cell of B and N atoms ($B_{20}N_{20}$) whose length is 5.038 Å. Unlike the nanosheet, the nanotube was expanded in one direction only. We optimized this cell using the 1D periodic boundary condition DFT method with the PBEPBE functional together with the basis set 6-311G (d). A 5 × 1 × 1k-point sampling in the Brillion zone was employed in such a way that, by increasing the number of unit cells, the gradient of the absolute value of the total dipole moment and the total energy became minimal. After the optimization of the pristine unit cell, we substituted Al and Ga with the B atom, and P and As with the N atom. Then, the optimization process was repeated for the doped nanotubes in order to study the effect of dopant through the adsorption process. To investigate the effect of nanotube length and diameter on the amount of adsorption energy, a number of calculations have been performed that these measurement results show that an increase in the length ($B_{30}N_{30}$, $B_{40}N_{40}$) of the nanotube and also an increase in its diameter, like armchair (7, 7), will not have a significant effect on the amount of adsorption energy. One reason could be the increase in the amount of deformation energy along with the increase in the diameter of the nanotube during the

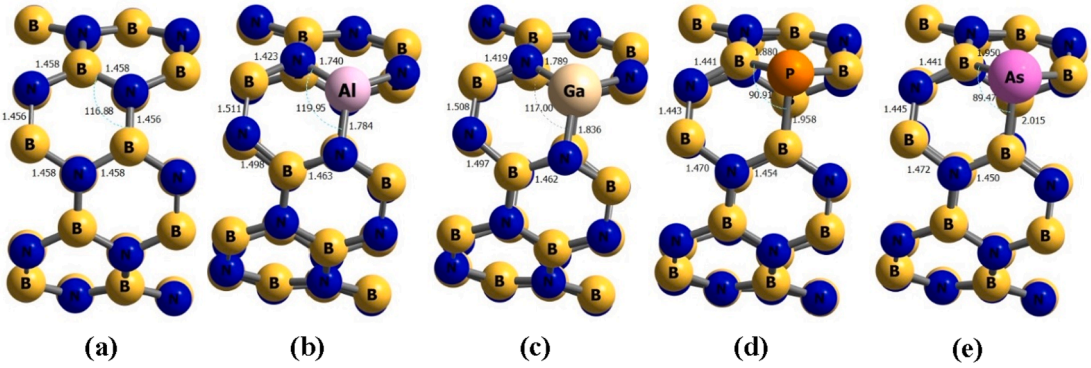

Fig. 1. Unit cell structures of the (a) BNNT, (b) BNAlNT, (c) BNGaNT, (d) BNPNT, and (e) BNAsNT systems. The optimization process was performed using the PBEPBE/6-311G (d) level of theory. All quantitative values are in angstrom (Å).

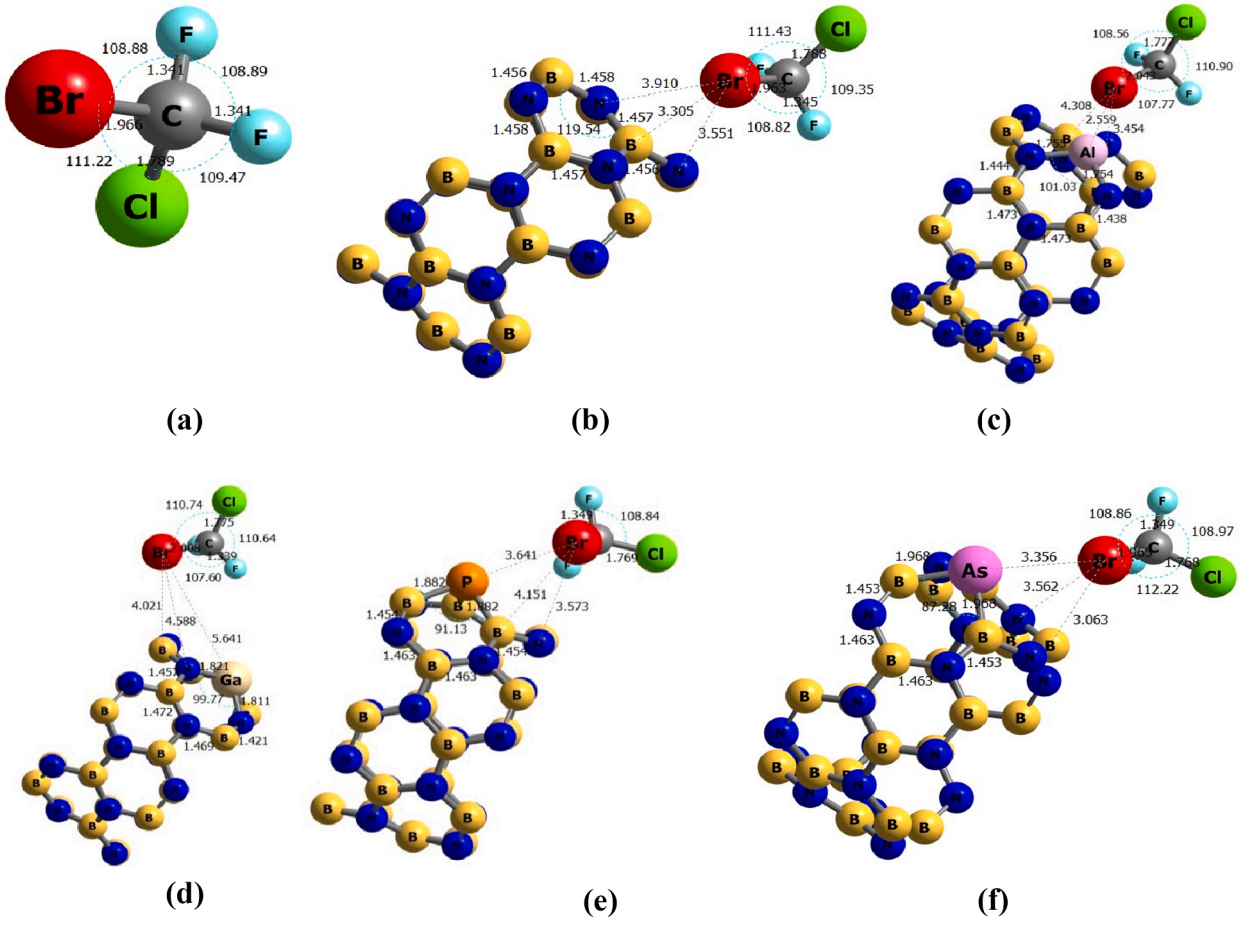

Fig. 2. The most stable form of (a) isolated BCF and adsorbed BCF molecule on the outer surface of (b) BNNT, (c) BNAlNT, (d) BNGaNT, (e) BNPNT, and (f) BNAsNT. All clusters were optimized using the PBEPBE functional and 6-311G (d) basis set. All quantitative values are in angstrom (Å).

adsorption process. Therefore, the selection of the $B_{20}N_{20}$ armchair (5, 5) nanotube is appropriate and logical in terms of computational costs. The quantitative bond lengths are shown in Fig. 1. Test results show that the changes in length and diameter of the nanotubes

The next step involved the optimization of the BCF/nanotube complexes. In this step, the BCF molecule was placed on the outer surface of each above-mentioned unit cell at a vertical distance of approximately 2.1 Å. To find the optimum distance between the nanotube and the BCF molecule, we used the rigid scan to estimate the most efficient distance for some cases. It should be noted that we used the PBEPBE/6-311G (d) level of theory for both the optimization and the rigid scan. To better explain the details of the adsorption process, compare Figs. 1 and 2.

Since the pure GGA functional does not account for the long-range dispersion contribution, it is expected that in poor interactions, this functional may not provide a good estimate of the amount of energy. For this reason, methods have been developed to calculate dispersion effects. One of the most effective, accurate and low computational methods is the experimental method developed by Grimme et al. Various versions of the semi-empirical Grimme method have been presented in recent years [46,47,58]. In this work we used the latest version of B3LYP-D3 known as D3 (BD) (GD3BJ) to reoptimize the structures due to dispertion consideration through optimization calculations. The

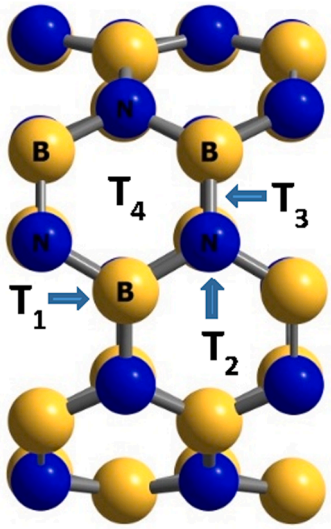

Fig. 3. All possible target positions for the adsorption of any arbitrary molecules onto the surface of BNNT. Top of the B atom (T_1), top of the N atom (T_2), between the B and N atoms (T_3), and top of the hexagonal ring (T_4).

results obtained from B3LYP-D3/6-311 g(d) repeated the same trend for adsorption energies (i.e. BCF/BN(Al)NT > BCF/BN(Ga)NT > BCF/BN (As)NT > BCF/BN(P)NT > BCF/BNNT).

The BNNT is composed of several symmetric hexagons with four different adsorption positions for the adsorption of any molecule onto the outer surface of the nanotube, as shown in Fig. 3: on the B atom (T_1), on the N atom (T_2), on the B-N bond (T_3), and at the hexagonal center (T_4). The logical approach is to place the BCF molecule in each of these positions and measure the amount of adsorption energy (E_{ads}). It is important to note that the BCF molecule has different heads (Br, Cl, and F), and that each of these heads must be placed at the desired position on the nanotube to measure the amount of adsorption energy. Our experience shows that negligible differences exist in the amounts of adsorption energies when we place the gas molecule in different directions on the nanotube. As mentioned in [59], when the differences in the adsorption energies are "below the range of chemical interest", placing the BCF molecule from different heads in different positions on the nanotubes provides identical results. To confirm this, we placed the BCF molecule from the Br head in the desired positions on the BN nanotube. The results showed negligible differences among the adsorption energies; therefore, the position of the B atom was chosen as the target position on the BN nanotube.

Next, we extended the unit cell to five units and terminated them with H atoms (Fig. 4). The nanotube length of $B_{100}N_{100}H_{20}$ increased to 27.193Å with the same diameter. The single-point energy calculations using different functionals (B3LYP, CAM-B3LYP, ωB97XD, and M06-2X, and the 6-311G (d) basis set) were performed. The calculated values indicated strong interactions between the nanotubes and the BCF molecule. In this work, we used CAM-B3LYP and ωB97XD to consider long-range and dispersion effects. The well-known B3LYP hybrid and M06-2X functionals were used to allow good comparisons. The results of the energy calculations of the systems studied using the above-mentioned levels of theory are reported in Table 1. The results show that the energies obtained from the PBEPBE and other functionals were consistent with the accuracy of the calculations. On the other hand, as expected, the ωB97XD method showed higher energy values due to the consideration of the contribution of dispersion. Moreover, doping the Al, Ga, P, and As elements on the BN nanotubes led to significant changes in the results. Table 1 shows that doping using As and P as well as Al and Ga increased the adsorption energy and enhanced the chemical adsorption.

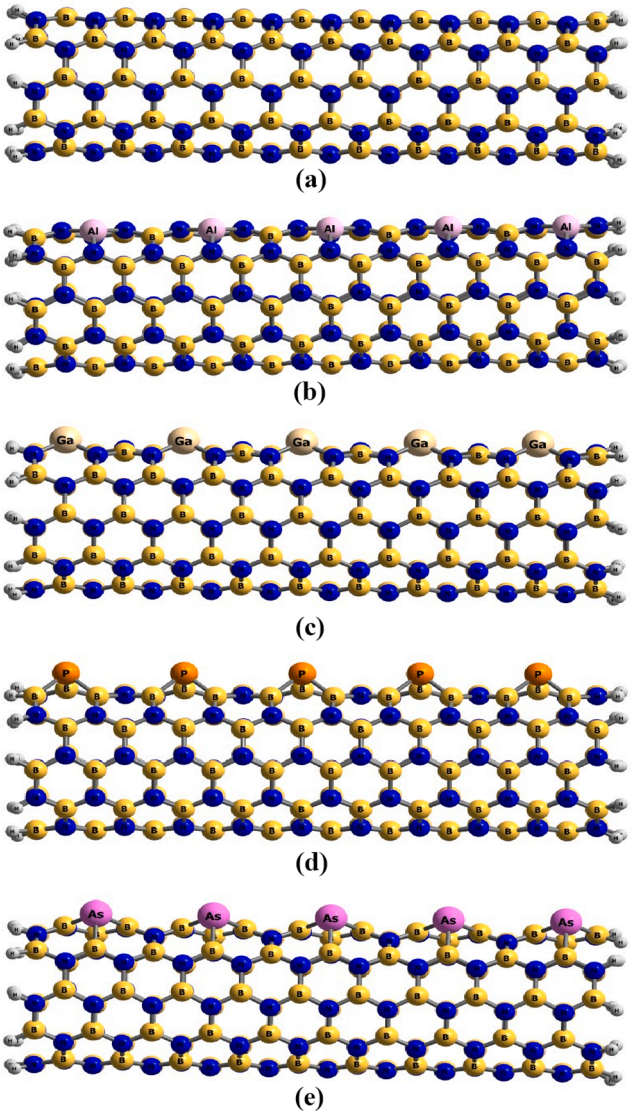

Fig. 4. Expanded (a) BN, (b) Al-doped BN, (c) Ga-doped BN, (d) P-doped BN, and (e) As-doped BNNTs terminated with H atoms.

Table 1
The adsorption energies (E_{ads}) for the nanotube and BCF molecule obtained from different functionals and 6-311 g(d) basis set. Units: eV.

Systems	Optimization		Single point			
	PBEPBE	B3LYP-D3	B3LYP	CAM-B3LYP	M06-2X	ωB97XD
$CBrClF_2$/BNNT	−1.513	−2.613	−1.12	−1.58	−2.522	−2.736
$CBrClF_2$/BN(Al)NT	−4.728	−5.565	−3.778	−4.218	−5.069	−5.425
$CBrClF_2$/BN(Ga)NT	−4.058	−4.457	−3.23	−3.62	−4.423	−4.718
$CBrClF_2$/BN(P)NT	−1.818	−3.121	−1.137	−1.75	−3.066	−3.082
$CBrClF_2$/BN(As)NT	−3.295	−4.389	−2.345	−2.998	−4.665	−4.518

3.2. Energetics properties

The values of the HOMO and LUMO, and their differences the HOMO–LUMO gap or (HLG), chemical potential (μ), chemical hardness (η), and electrophilicity (ω) are reported in Table 2. It can be seen that

Table 2
HOMO energy (ε_H), LUMO energy (ε_L), HOMO–LUMO energy gap (HLG), chemical potential (μ), chemical hardness (η), and electrophilicity (ω). All values are in eV and were obtained using the PBEPBE/6-311G (d) level of theory.

Systems	ε_H	ε_L	HLG	μ	η	ω
BNNT	−5.578	−1.086	4.492	−3.332	2.246	12.468
BN(Al)NT	−5.452	−2.327	3.125	−3.889	1.563	11.820
BN(Ga)NT	−5.392	−2.944	2.448	−4.168	1.224	10.630
BN(P)NT	−5.542	−2.070	3.472	−3.806	1.736	12.576
BN(As)NT	−5.364	−2.131	3.233	−3.747	1.616	11.349
$CBrClF_2$/BNNT	−5.546	−2.384	3.162	−3.965	1.581	12.427
$CBrClF_2$/BN(Al)NT	−4.971	−4.119	0.852	−4.545	0.426	4.400
$CBrClF_2$/BN(Ga)NT	−5.110	−3.814	1.296	−4.462	0.648	6.449
$CBrClF_2$/BN(P)NT	−5.510	−2.360	3.150	−3.935	1.575	12.194
$CBrClF_2$/BN(As)NT	−5.350	−2.323	3.027	−3.837	1.513	11.140

adsorption of the BCF molecule onto the outer surface of the nanotubes reduced the distance between the HOMO and LUMO levels relative to the corresponding value for the pure nanotube. The greatest decrease was observed in the interaction of the Al-doped BNNT and BCF, which can be attributed to the molecular energy adsorption matching this position. Doping with Al, Ga, P, and As decreased HLG. The decrease in HLG increased the electrical conductivity, thereby increasing the metal properties of all the nanotubes compared to the case of the pure BNNT. Moreover, note that the observed changes in HLG after doping with Al, Ga, P, and As were mainly due to the lower LUMO energy levels, and these changes were greater for metallic elements than the non-metallic ones. After the adsorption of BCF, HLG of the nanotubes doped with Al and Ga increased, whereas it decreased for the nanotubes doped with non-metallic elements (P and As). The electrical conductivity is proportional to the exponentially relationship to the energy gap [60] as sollows:

$$\sigma \propto T^{3/2} e^{\frac{E_g}{2kT}} \tag{7}$$

where k is the Boltzmann's constant and T is absolute temperature and Eg shows the energy gap. Owing to the remarkable HLG decrease through adsorption process, if the nanotubes are assumed as a part of an electric circuit, they can make an electrical signal, according to the magnitude order of energy gap decrease after the adsorption process. In order to study these changes in the electron structures more closely, the density of state (DOS) spectra were analyzed (Fig. 5). It means The DOS spectra can be estimated the energy gap of molecular structures [61] (see Figs. 6 and 7).

The DOS spectra for all the adsorptions agree with the values of the energy parameters reported in Table 2. The lowest adsorption energy occurred for the pristine nanotube, and the highest, for the adsorption of BCF onto the Al-doped BN nanotube. The majority of the changes were also observed in the DOS spectrum relative to the Al-doped nanotube. In other words, the changes in the electron structure showed a direct relationship with the adsorption energies. Given the amount of adsorption energy, high binding energy, and structures of the DOS spectra obtained in all the cases, it is logical to conclude that the adsorption of the BCF molecule onto the BN, BN(Al), BN(Ga), BN(P), and BN (As) nanotubes was chemical in nature. In other words, the electronic transfers were significant.

3.3. NBO analysis

We used NBO analysis using the PBEPBE functional together with the 6-311g (d) basis set to perform the NBO calculations. The main idea behind natural atomic orbital (NAO) and NBO was developed by Weinhold et al. [62]. The concept of bonded orbitals can be used to understand the distribution of electrons in atomic and molecular orbitals. Atomic charges and molecular bonds can be used to obtain these orbitals. NBO is defined as the following equation for σ bonding between atoms A and B.

$$\sigma_{AB} = C_A h_A + C_B h_B \tag{8}$$

where h_A and h_B are natural hybrids on the A and B atoms. In the covalent limit, $C_A = C_B$, and at the ionic limit, $C_A \gg C_B$ (if the electronegativity of A is greater than B). Each bonding NBO must be paired with a corresponding anti-bonding NBO.

$$\sigma^*_{AB} = C_A h_A - C_B h_B \tag{9}$$

NBO analysis was used to calculate the bond order using the Wiberg method for a more detailed examination of the types of interactions. The following section presents these results. After studying the adsorption energy of the complexes, we examine the bond length and bond order of the molecule and the nanotube before and after the adsorption as well as by doping with the various elements. The bond length and bond order for these clusters are reported in Tables 3 and 4. According to these tables, the length of the B-N bond increased after the molecule adsorbed onto the nanotube, indicating that adsorption occurred between the molecule and the nanotube, and the bond order decreased as well.

After the elements were doped, the bond length between the doped element and the nanotube changes so that the system is in equilibrium. Table 3 shows the bond length of the nanotube doped with Al, Ga, P, and As after interaction with the BCF molecule. It is evident that the bond length increases by doping the elements. The increase in the bond length can be attributed to the increase in the atomic radius of the doped elements, because the doping atoms are larger than the N and B atoms.

The WBI relates to the bond order properties: the larger the WBI, the stronger the covalent character. As per the results in Table 3, the strongest bond occurs between the B atom from the BCF molecule and the Al atom from the BNAlNT, and this result agrees well with the previously presented results on adsorption energy.

The results of the NBO calculations shed light on the natural electron configuration and partial natural charge, which are useful in the study of the character of the bond between the nanotubes and the BCF molecule. The NBO approach was implemented for all atoms in the pristine and doped cluster systems to reveal the quantities listed in Table 5. For semiconducting inorganic nanotubes, such as those selected in this study, the negative charges located on the atom possess more electronegativity. The charge transfer quantity between the BCF molecule and the nanotubes can also be used as a criterion to study the interactions between the nanotubes and BCF, such that the stronger the interaction, the higher the charge transfer between the BCF and the nanotube. Table 5 shows that significant charge transfer must have occurred between the two species during the adsorption process.

In addition, the type of interaction between the nanotubes and BCF molecule can be described by implementing the natural electron configuration. The results in Table 5 clearly indicate that the valance configuration of the isolated BCF molecule and nanotubes as well as the valence configurations of the nanotube/BCF clusters increased. Therefore, the interactions of BCF with all the nanotubes can be classified as strong chemisorption.

The electron donor–acceptor electron configuration of the pristine BNNT and doped BN(Al), BN(Ga), BN(P), and BN(As) nanotubes are reported in Table 6. The most important interactions in terms of the electron transfer stability energies are reported. The existence of such interactions with the remarkable stability energies in this table shows that in all cases the doped atom was incorporated into the nanotube structure by chemical interaction, and a stable structure was created. In other words, the inserted atom behaved as a doping atom. The data in Table 6 show the most important interaction for the pristine nanotube, namely the electron transfer from the BD (B-N) bond as the electron donor to the BD* (C-Br) bond as the receptor. This finding agrees with the results of the adsorption energy as well as the other results examined thus far. The study of the doped complexes reveals that in the Al complex, the Al electron pair is the Al receptor (Lewis acid), and the *N*-

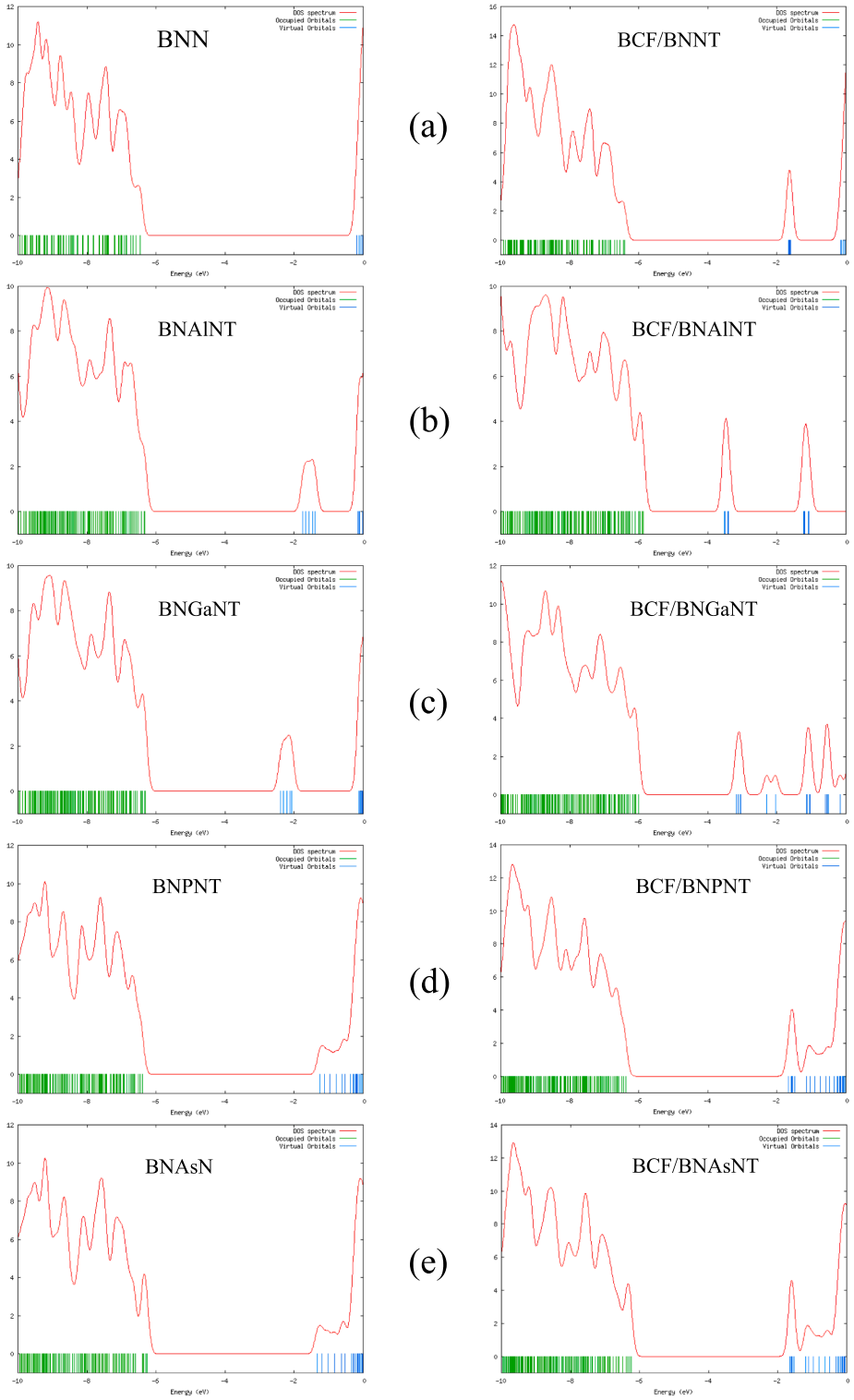

Fig. 5. DOS diagrams for the adsorption of BCF molecule onto the surface of (a) pristine (b) Al-doped, (c) Ga-doped, (d) P-doped, and (e) As-doped BNNTs. The data were obtained from completed nanotubes using the PBEPBE/6-311G (d) level of theory. The left panel shows isolated nanotubes, while the right panel shows BCF/nanotube clusters.

bonded electron pair is the amino group of the electron donor molecule (Lewis base). The highest electron–acceptor stabilization energy in all cases is due to the same interaction, which indicates the strong adsorption of the molecule onto the BN(Al) nanotube compared to the other cases.

3.4. QTAIM analysis

QTAIM is a powerful tool for studying the type and structure of bonds and intermolecular interactions. According to this theory, the critical point of the electron density, which can be a minimum point, a maximum point, or a saddle point, can fall into one of the following four

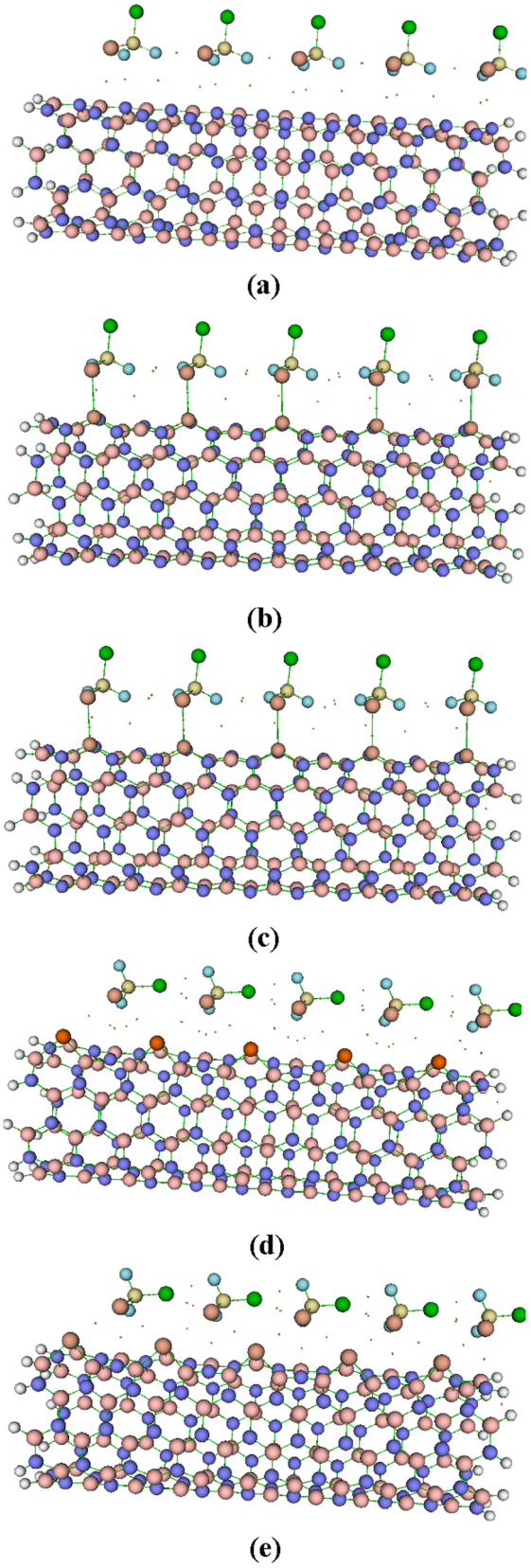

Fig. 6. QTAIM molecular graphs for the (a) BCF/BNNT, (b) BCF/BNAlNT, (c) BCF/BNGaNT, (d) BCF/BNPNT, and (e) BCF/BNAsNT systems. The orange dots represent the BCPs.

categories: (1) Atomic *critical point* (ACP); (2) bond *critical point* (BCP); (3) ring *critical point* (RCP); and (4) cage *critical point* (CCP).

The BCP with negative values of $\nabla^2\rho(r)$ and large values of $\rho(r)$ (of orders exceeding 10–1 a.u.) is defined as a shared (covalent) intermolecular interaction. Also, when $\nabla^2\rho(r)$ is positive, the interactions can be classified as of the non-substrate close-shell type (which include ionic and van der Waals interactions) [63]. The elliptical bond (ε) [64] and the virial theorem [65] are two other important factors in the classification of bonds. An elliptical bond represents the electron density preferentially accumulated on a plate containing the bond and is defined as follows:

$$\varepsilon = \frac{\lambda_1}{\lambda_2} - 1 \quad \text{where } |\lambda_1| > |\lambda_2| \tag{10}$$

Large values of ε indicate an unstable structure and vice versa. Also, based on the virial theorem, the following relationship exists between the electron kinetic energy density $G(r)$, the electron potential energy density $V(r)$, and $\nabla^2\rho(r)$:

$$\frac{1}{4}\nabla^2\rho(r) = 2G(r) + V(r) \tag{11}$$

The balance between $G(r)$ and $V(r)$ reflects the nature of the interaction, and therefore, the ratio of $G/|V|$ can be used as an appropriate index in link classification. If this ratio is<0.5, the nature of the interaction will be purely covalent, and if the ratio is greater than 1, the interaction may be considered as completely non-covalent. Note that for covalent bonds (i.e. $\nabla^2\rho(r) < 0$ and $G/|V| < 0.5$), the nature of the bond from van der Waals interactions to strong covalent interactions. It becomes covalent. It can also play a decisive role in controlling the amount of ionic interaction for close-shell interactions (i.e. $\nabla^2\rho(r) > 0$ and $G/|V| > 1$), as they become stronger ionically (and weakly electrostatic) by reducing interactions. The information obtained after optimizing the initial and doped nanotubes and their complexes using QTAIM analysis is reported in Table 7.

Table 7 shows important results. All the adsorption sites had pposi-tive values for the Laplacian of electron energy density (i.e. the bonds are non-covalent). The study of the doped systems showed that the energy densities and the Laplacian of electron energy densities were high for all clusters, indicating that a strong bond exists between the nanotubes and the BCF molecule, and the elliptical bond is close to 0. Thus, the interaction is strong. As stated above, when $G/|V|$ exceeds 1, the bond is non-covalent, and in the case of Al- and Ga-doped clusters, these amounts are less than 1. In other words, the results of the QTAIM analysis also confirm the chemical adsorption of the BCF molecule on BN (Al)NT and BN(Ga)NT.

The averaged reduced density gradient (RDG) method is another powerful way to analyze the types of intermolecular interactions, and it is defined as follows [66,67]:

$$RDGs = \frac{1}{2(3\pi^2)^{\frac{1}{3}}} \frac{|\overline{\Delta\rho}(r)|}{\overline{\rho(r)}^{\frac{4}{3}}} \tag{12}$$

The strength of the interaction has a positive correlation with electron density $\rho(r)$ and the second largest eigenvalue of the Hessian matrix (λ_2). Thus, the real space function sign of $\lambda_2(r)\rho(r)$ (the products of the signs of λ_2 and ρ) can be defined. The scatter graph of the sign of the $\lambda_2(r)\rho(r)$ function (X-axis) and RDG (Y-axis) reveals the interaction type between gases and nanocages. The RDG values range from medium to very large around the nuclei and edges of the molecules, whereas weak interactions (zero to medium) are observed around the chemical bonds. Also, for each specific value of RDG (seen as a horizontal line on the graph), the regions of the graph can be classified into three types, namely, Sign$\lambda_2(r)\rho(r) < 0$ (strong attraction), sign$\lambda_2(r)\rho(r) \approx 0$ (weak van der Waals interaction), and sign$\lambda_2(r)\rho(r) > 0$ (strong repulsion (steric effect in ring)) [66,67].

Using the isosurface RDG = 0.5 as a reference, it can be concluded

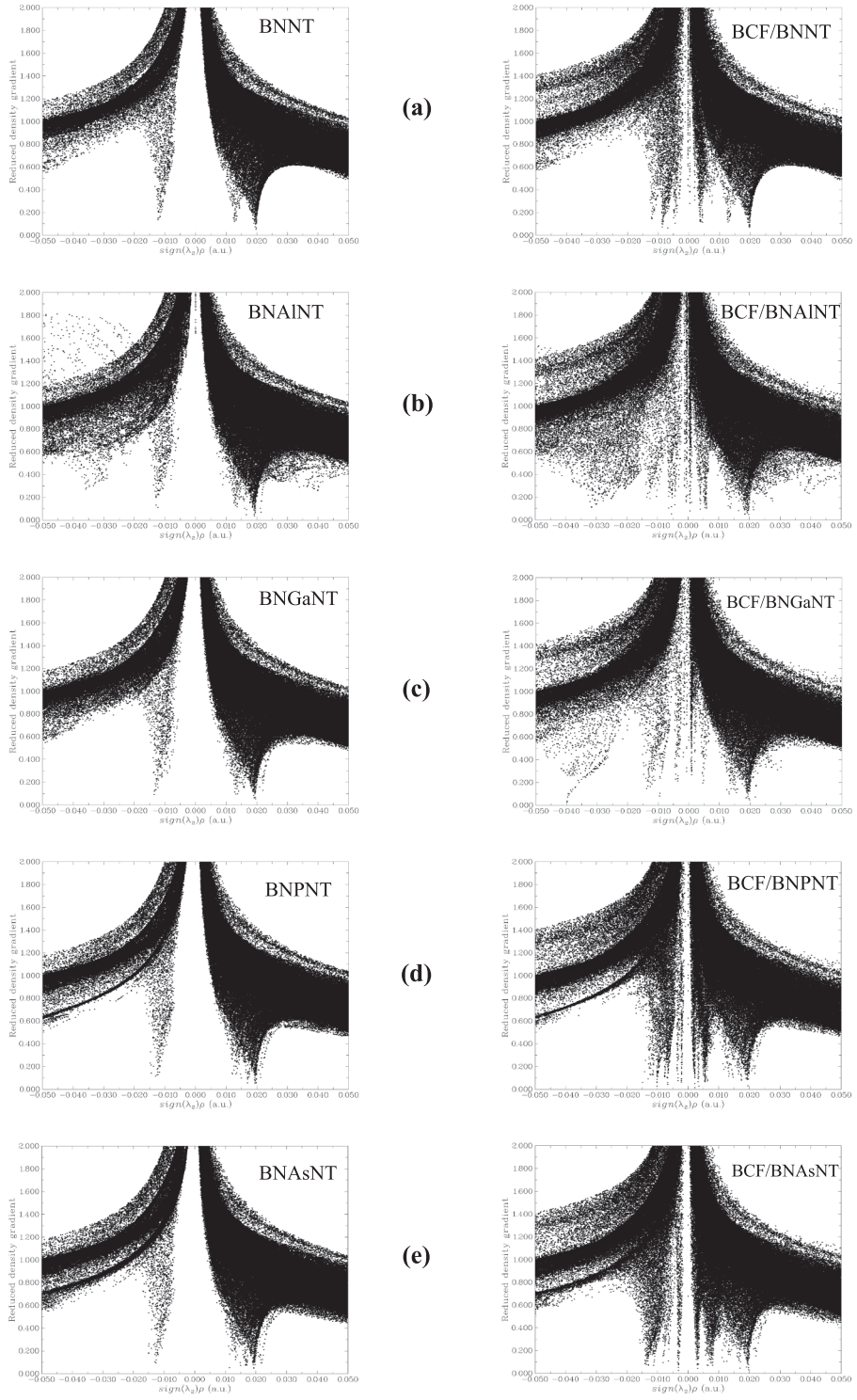

Fig. 7. Plots for the reduced density gradient (RDG) vs. sign(λ_2)ρ(r) values of the (a) pristine (b) Al-doped, (c) Ga-doped, (d) P-doped, and (e) As-doped BNNTs. The data were obtained from completed nanotubes and using the PBEPBE/6-311G (d) level of theory. The diagrams in the left panel show isolated nanotubes, and those in the right panel are BCF/nanotube clusters.

that after adsorption of the BCF molecule onto the outer surfaces of the nanotubes, spots appeared around the region characterized by sign$\lambda_2(r)\rho(r) \approx 0$. The interactions of BCF with the nanotubes were strong and intermolecular in nature. Significant changes in the overall features of the pristine nanotubes graph after the adsorption of BCF were observed in the region characterized as sign$\lambda_2(r)\rho(r) < 0$ (i.e. strong attraction), implying that the nanotube/BCF interactions were stronger compared with those of the isolated nanotubes. Hence, this analysis also confirms the results of the single-point energy calculations and NBO analysis, namely that the interactions of BCF with the pristine and doped nanotubes were strong.

Table 3
Bond lengths and nearest intermolecular distances (re (Å)) between the BCF molecule and BNNT, BNAlNT, BNGaNT, BNPNT, and BNAsNT. All calculations were performed using the PBC-DFT PBEPBE/6-311G (d) level of theory.

r_e (Å)	Br···(x)	Br···B	Br···N	C···(x)	Cl···(x)	F···(x)
$CBrClF_2$/BNNT	–	3.305	3.551	–	–	–
$CBrClF_2$/BN(Al)NT	2.559	4.308	3.454	3.587	5.226	3.7524
$CBrClF_2$/BN(Ga)NT	5.641	4.021	4.588	5.283	6.856	4.3089
$CBrClF_2$/BN(P)NT	3.641	4.151	3.573	5.137	6.497	5.0235
$CBrClF_2$/BN(As)NT	3.356	3.063	3.362	4.930	6.30953	4.922

Table 4
WBI obtained for atomic bonds and intermolecular interactions between the BCF molecule and BNNT, BNAlNT, BNGaNT, BNPNT, and BNAsNT. All calculations were performed using the PBEPBE/6-311G (d) level of theory.

WBI	Br···(x)	Br···B	Br···N	C···(x)	Cl···(x)	F···(x)
$CBrClF_2$/BNNT	–	0.037	0.005	–	–	–
$CBrClF_2$/BN(Al)NT	0.379	0.002	0.023	0.003	0.009	0.0060
$CBrClF_2$/BN(Ga)NT	0.360	0.003	0.032	0.004	0.007	0.0184
$CBrClF_2$/BN(P)NT	0.011	0.055	0.006	0.003	0.001	0.0002
$CBrClF_2$/BN(As)NT	0.029	0.082	0.009	0.009	0.002	0.0005

Table 5
Natural electron configurations and natural charges (au) for the isolated BCF, pristine and Al-, Ga-, P-, and As-doped nanotubes, and their complex structures. All values were calculated using the PBEPBE/6-311G (d) level of theory.

Systems	Atom	Natural Charge	Natural Electron Configuration
BNNT	B	1.14	[core]2S(0.45)2p(1.40)3p(0.01)3d(0.01)
	N	−1.14	[core]2S(1.35)2p(4.78)
BN(Al)NT	B	1.12	[core]2S(0.46)2p(1.41)3p(0.01)3d(0.01)
	N	−1.14	[core]2S(1.41)2p(4.93)3p(0.01)
	Al	1.96	[core]3S(0.44)3p(0.57)3d(0.02)4p(0.01)
BN(Ga)NT	B	1.14	[core]2S(0.46)2p(1.42)3p(0.01)3d(0.01)
	N	−1.31	[core]2S(1.40)2p(4.88)3p(0.01)
	Ga	1.72	[core]4S(0.63)4p(0.67)4d(0.01)5p(0.01)
BN(P)NT	B	1.12	[core]2S(0.46)2p(1.40)3p(0.01)3d(0.01)
	N	−1.14	[core]2S(1.36)2p(4.77)
	P	0.18	[core]3S(1.42)3p(3.42)3d(0.02)4p(0.01)
BN(As)NT	B	1.14	[core]2S(0.46)2p(1.40)3p(0.01)3d(0.01)
	N	−1.13	[core]2S(1.36)2p(4.77)
	As	0.25	[core]4S(1.47)4p(3.31)4d(0.01)5p(0.01)
$CBrClF_2$/BNNT	B	1.14	[core]2S(0.45)2p(1.39)3p(0.01)3d(0.01)
	N	−1.14	[core]2S(1.35)2p(4.78)
	C	0.54	[core]2S(1.00)2p(2.39)3S(0.01)3p(0.05)3d(0.02)
	Br	0.08	[core]4S(1.90)4p(5.00)4d(0.01)5p(0.01)
	Cl	0.01	[core]3S(1.87)3p(5.10)3d(0.01)4p(0.01)
	F	−0.30	[core]2S(1.84)2p(5.45)3d(0.01)
$CBrClF_2$/BN(Al)NT	B	1.14	[core]2S(0.45)2p(1.39)3p(0.01)3d(0.01)
	N	−1.14	[core]2S(1.35)2p(4.78)
	Al	1.83	[core]3S(0.45)3p(0.69)3d(0.03)4p(0.01)
	C	0.59	[core]2S(0.98)2p(2.36)3S(0.01)3p(0.05)3d(0.02)
	Br	0.12	[core]4S(1.86)4p(5.00)4d(0.01)
	Cl	0.04	[core]3S(1.86)3p(5.08)3d(0.01)4p(0.01)
	F	−0.27	[core]2S(1.83)2p(5.43)3d(0.01)
$CBrClF_2$/BN(Ga)NT	B	1.14	[core]2S(0.45)2p(1.39)3p(0.01)3d(0.01)
	N	−1.14	[core]2S(1.35)2p(4.78)
	Ga	1.61	[core]4S(0.64)4p(0.75)4d(0.01)5p(0.01)
	C	0.56	[core]2S(0.99)2p(2.38)3S(0.01)3p(0.05)3d(0.02)
	Br	0.19	[core]4S(1.86)4p(4.93)4d(0.01)5p(0.01)
	Cl	0.04	[core]3S(1.86)3p(5.07)3d(0.01)4p(0.01)
	F	−0.29	[core]2S(1.84)2p(5.45)3d(0.01)
$CBrClF_2$/BN(P)NT	B	1.14	[core]2S(0.45)2p(1.40)3p(0.01)3d(0.01)
	N	−1.14	[core]2S(1.36)2p(4.77)
	P	0.15	[core]3S(1.40)3p(3.43)3d(0.01)4p(0.01)
	C	0.52	[core]2S(1.00)2p(2.40)3S(0.01)3p(0.05)3d(0.02)
	Br	0.11	[core]4S(1.89)4p(4.98)4d(0.01)5p(0.01)
	Cl	0.03	[core]3S(1.86)3p(5.09)3d(0.01)4p(0.01)
	F	−0.30	[core]2S(1.84)2p(5.45)3d(0.01)
$CBrClF_2$/BN(As)NT	B	1.14	[core]2S(0.60)2p(1.68)3p(0.02)3d(0.01)
	N	−1.14	[core]2S(1.36)2p(4.78)
	As	0.21	[core]4S(1.46)4p(3.32)4d(0.01)
	C	0.52	[core]2S(1.00)2p(2.40)3S(0.01)3p(0.05)3d(0.02)

(*continued on next page*)

Table 5 (*continued*)

Systems	Atom	Natural Charge	Natural Electron Configuration
	Br	0.12	[core]4S(1.89)4p(4.96)4d(0.01)5p(0.01)
	Cl	0.03	[core]3S(1.86)3p(5.09)3d(0.01)4p(0.01)
	F	−0.30	[core]2S(1.84)2p(5.46)3d(0.01)
$CBrClF_2$	C	0.54	[core]2S(1.00)2p(2.39)3S(0.01)3p(0.05)3d(0.02)
	Br	0.05	[core]4S(1.90)4p(5.03)4d(0.01)5p(0.01)
	Cl	0.01	[core]3S(1.87)3p(5.11)3d(0.01)4p(0.01)
	F	−0.30	[core]2S(1.84)2p(5.45)3d(0.01)

Table 6
Donor–acceptor NBO interactions and second-order perturbation energies (E^2) for BCF clusters with BNNT, BNAlNT, BNGaNT, BNPNT, and BNAsNT. All values were obtained from the completed nanotubes using the PBEPBE/6-311G (d) level of theory.

Systems	Donor NBO (i)	Acceptor NBO (j)	E2(kcal/mol)
$CBrClF_2$/BNNT	BD (B-N)	BD*(C-Br)	0.09
	BD (B-N)	BD*(C-Cl)	0.08
	BD (B-N)	BD*(C-F)	0.06
	BD (B-N)	RY*(Br)	0.06
	BD (B-N)	RY*(C)	0.05
$CBrClF_2$/BN(Al)NT	BD (B-N)	BD*(C-Br)	0.11
	BD (B-N)	BD*(C-F)	0.06
$CBrClF_2$/BN(Ga)NT	BD (B-Ga)	BD*(C-Br)	0.8
	BD (B-N)	RY*(Br)	0.4
$CBrClF_2$/BN(P)NT	BD (B-N)	BD*(C-Br)	0.07
	BD (B-N)	RY*(Br)	0.05
$CBrClF_2$/BN(As)NT	BD (B-As)	BD*(C-Br)	0.1
	BD (B-N)	BD*(C-Br)	0.09
	BD (B-N)	RY*(Br)	0.09

Table 7
QTAIM topological parameters (electron density (ρ(r)), Laplacian of electron density ($\nabla^2\rho(r)$), kinetic electron density G(r), potential electron density V(r), eigenvalues of Hessian matrix (λ), and bond ellipticity index (ε)) at the BCPs of the BCF clusters with BNNT, BNAlNT, BNGaNT, BNPNT, and BNAsNT. All values were calculated using the PBEPBE/6-311G (d) level of theory and NBO analysis.

Systems	Bond	ρ	$\nabla^2 r$	G(r)	V(r)	G(r)/V(r)	λ_1	λ_2	λ_3	ε
CBrClF2/BNNT	Br···N	0.0088	0.0244	0.0052	−0.0042	1.2203	−0.0046	0.0313	−0.0023	1.0641
CBrClF2/BN(Al)NT	Br···Al	0.0317	0.0852	0.0264	−0.0315	0.8379	−0.0271	0.1355	−0.0232	0.1670
CBrClF2/BN(Ga)NT	Br···Ga	0.0399	0.0903	0.0295	−0.0364	0.8100	−0.0312	0.1547	−0.0332	0.0651
CBrClF2/BN(P)NT	Br···P	0.0102	0.0258	0.0057	−0.0048	1.1668	−0.0054	0.0351	−0.0038	0.4223
CBrClF2/BN(As)NT	Br···As	0.0113	0.0292	0.0061	−0.0050	1.2341	−0.0065	0.0417	−0.0059	0.1056

4. Conclusion

In this study, the interactions between BCF molecules and pristine, Al-, Ga-, P-, and As-doped BNNTs were investigated using the density functional framework. The structures of the nanotubes and BCF molecule were optimized using the PBEPBE/6-311G (d) level of theory. The B3LYP, CAM-B3LYP, M06-2X, and ωB97XD functionals and the same basis set were also used to consider the contribution of long-range interactions and the dispersion effect. QTAIM and NBO analyses were implemented to consider the characteristics of the intermolecular interactions. The results of all the analyses were in agreement, and showed the following: (1) Among the different positions studied for pristine BNNT, position T_1 had the highest adsorption energy. (2) Al, Ga, P, and As can be substituted by BNNT atoms via chemical bonding, and as binding elements, they can cause dramatic changes in the chemical, electronic, and mechanical structures of the BNNT nanotubes. (3) Among the doped nanotubes, Al-doped BNNT showed a very high adsorption energy compared to those of BNNT doped with other elements. The interaction is chemical adsorption in this case, making this doped BNNT a suitable sensor option. The next category concerns Ga, for which the adsorption energy is higher than the initial state but lower than that of Al. Also, due to their strong adsorption, the As- and P-doped nanotubes may be better options than the pure BN nanotubes for designing suitable BCF nanosensors.

CRediT authorship contribution statement

Mohsen Doust Mohammadi: Investigation, Writing - original draft. **Hewa Y. Abdullah:** Conceptualization, Writing - review & editing, Resources, Supervision.

Declaration of Competing Interest

The authors declare that they have no known competing financial interests or personal relationships that could have appeared to influence the work reported in this paper.

Acknowledgements

I would like to thank the Solid-State Theory Group at the Physics Department at the Universita‘ degli Studi di Milano-Italy for providing computational facilities.

References

[1] M. Monthioux, V.L. Kuznetsov, Who should be given the credit for the discovery of carbon nanotubes? Carbon 44 (2006) 1621–1623.
[2] M. Ghadamgahi, D. Ajloo, Molecular dynamics insight into the urea effect on Tretinoin encapsulation into carbon nanotube, J. Brazil. Chem. Soc. 26 (2015) 185–195.
[3] W. Wu, S. Wieckowski, G. Pastorin, M. Benincasa, C. Klumpp, J.P. Briand, R. Gennaro, M. Prato, A. Bianco, Targeted delivery of amphotericin B to cells by using functionalized carbon nanotubes, Angew. Chem. Int. Ed. 44 (2005) 6358–6362.
[4] L. Wang, D. Zhu, L. Duan, W. Chen, Adsorption of single-ringed N-and S-heterocyclic aromatics on carbon nanotubes, Carbon 48 (2010) 3906–3915.
[5] V. Rastogi, P. Yadav, S.S. Bhattacharya, A.K. Mishra, N. Verma, A. Verma, J. K. Pandit, Carbon nanotubes: an emerging drug carrier for targeting cancer cells, J. Drug Deliv. 2014 (2014).
[6] N.G. Chopra, L.X. Benedict, V.H. Crespi, M.L. Cohen, S.G. Louie, A. Zettl, Fully collapsed carbon nanotubes, Nature 377 (1995) 135–138.
[7] W.-Q. Han, W. Mickelson, J. Cumings, A. Zettl, Transformation of B x C y N z nanotubes to pure BN nanotubes, Appl. Phys. Lett. 81 (2002) 1110–1112.
[8] D. Golberg, Y. Bando, C. Tang, C. Zhi, Boron nitride nanotubes, Adv. Mater. 19 (2007) 2413–2432.
[9] X. Blase, A. Rubio, S. Louie, M. Cohen, Stability and band gap constancy of boron nitride nanotubes, EPL (Europhysics Letters) 28 (1994) 335.
[10] K.M. Liew, J. Yuan, High-temperature thermal stability and axial compressive properties of a coaxial carbon nanotube inside a boron nitride nanotube, Nanotechnology 22 (2011) 085701.
[11] D. Golberg, Y. Bando, K. Kurashima, T. Sato, Synthesis and characterization of ropes made of BN multiwalled nanotubes, Scr. Mater. 44 (2001) 1561–1565.
[12] S.M. Nakhmanson, A. Calzolari, V. Meunier, J. Bernholc, M.B. Nardelli, Spontaneous polarization and piezoelectricity in boron nitride nanotubes, Phys. Rev. B 67 (2003) 235406.
[13] C. Chang, A. Fennimore, A. Afanasiev, D. Okawa, T. Ikuno, H. Garcia, D. Li, A. Majumdar, A. Zettl, Isotope effect on the thermal conductivity of boron nitride nanotubes, Phys. Rev. Lett. 97 (2006) 085901.
[14] Q. Weng, B. Wang, X. Wang, N. Hanagata, X. Li, D. Liu, X. Wang, X. Jiang, Y. Bando, D. Golberg, Highly water-soluble, porous, and biocompatible boron nitrides for anticancer drug delivery, ACS Nano 8 (2014) 6123–6130.
[15] G. Ciofani, S. Danti, S. Nitti, B. Mazzolai, V. Mattoli, M. Giorgi, Biocompatibility of boron nitride nanotubes: an up-date of in vivo toxicological investigation, Int. J. Pharm. 444 (2013) 85–88.
[16] G. Ciofani, V. Raffa, A. Menciassi, A. Cuschieri, Cytocompatibility, interactions, and uptake of polyethyleneimine-coated boron nitride nanotubes by living cells: confirmation of their potential for biomedical applications, Biotechnol. Bioeng. 101 (2008) 850–858.
[17] G. Ciofani, V. Raffa, A. Menciassi, A. Cuschieri, Folate functionalized boron nitride nanotubes and their selective uptake by glioblastoma multiforme cells: implications for their use as boron carriers in clinical boron neutron capture therapy, Nanoscale Res. Lett. 4 (2009) 113.
[18] C. Zhi, Y. Bando, C. Tang, D. Golberg, Boron nitride nanotubes, Mater. Sci. Eng.: R: Reports 70 (2010) 92–111.
[19] A. Rubio, J.L. Corkill, M.L. Cohen, Theory of graphitic boron nitride nanotubes, Phys. Rev. B 49 (1994) 5081.
[20] N.G. Chopra, R. Luyken, K. Cherrey, V.H. Crespi, M.L. Cohen, S.G. Louie, A. Zettl, Boron nitride nanotubes, Science 269 (1995) 966–967.
[21] N. Saikia, S.K. Pati, R.C. Deka, First principles calculation on the structure and electronic properties of BNNTs functionalized with isoniazid drug molecule, Appl. Nanosci. 2 (2012) 389–400.
[22] S. Mukhopadhyay, R.H. Scheicher, R. Pandey, S.P. Karna, Sensitivity of boron nitride nanotubes toward biomolecules of different polarities, J. Phys. Chem. Lett. 2 (2011) 2442–2447.
[23] A.A. Peyghan, M.T. Baei, M. Moghimi, S. Hashemian, Adsorption and electronic structure study of imidazole on (6, 0) zigzag single-walled boron nitride nanotube, J. Cluster Sci. 24 (2013) 31–47.
[24] C.-K. Yang, Exploring the interaction between the boron nitride nanotube and biological molecules, Comput. Phys. Commun. 182 (2011) 39–42.
[25] E.C. Anota, G.H. Cocoletzi, GGA-based analysis of the metformin adsorption on BN nanotubes, Physica E 56 (2014) 134–140.
[26] M. Mirzaei, Uracil-functionalized ultra-small (n, 0) boron nitride nanotubes (n= 3–6): computational studies, Superlattices Microstruct. 57 (2013) 44–50.
[27] M. Abbasi, E. Nemati-Kande, M.D. Mohammadi, Doping of the first row transition metals onto B12N12 nanocage: a DFT study, Comput. Theor. Chem. 1132 (2018) 1–11.
[28] M.D. Mohammadi, M. Hamzehloo, The adsorption of bromomethane onto the exterior surface of aluminum nitride, boron nitride, carbon, and silicon carbide nanotubes: a PBC-DFT NBO, and QTAIM study, Comput. Theoret. Chem. 1144 (2018) 26–37.
[29] E. Nemati-Kande, M. Abbasi, M. Doust Mohammadi, DFT, QTAIM and NBO investigation of the interaction of rare gases with pristine and decorated boron nitride nanotube, ChemistrySelect 3 (2018) 9833–9840.
[30] E. Nemati-Kande, M. Abbasi, M.D. Mohammadi, Feasibility of pristine and decorated AlN and SiC nanotubes in sensing of noble gases: a DFT study, ChemistrySelect 4 (2019) 2453–2462.
[31] Z. Mahdavifar, Z. Nomresaz, E. Shakerzadeh, Hetero-fullerenes C59M (M= B, Al, Ga, Ge, N, P, As) for sulfur dioxide gas sensing: computational approach, Chem. Phys. 530 (2020) 110606.
[32] N. Mohammadi-rad, M.D. Esrafili, J.J. Sardroodi, CuN3 doped graphene as an active electrocatalyst for oxygen reduction reaction in fuel cells: a DFT study, J. Mol. Graph. Model. (2020) 107537.
[33] E. Nemati-Kande, M. Abbasi, M.D. Mohammadi, DFT studies on the interactions of pristine, Al and Ga-doped boron nitride nanosheets with CH3X (X= F, Cl and Br), J. Mol. Struct. 1199 (2020) 126962.
[34] E. Nemati-Kande, R. Karimian, V. Goodarzi, E. Ghazizadeh, Feasibility of pristine, Al-doped and Ga-doped boron nitride nanotubes for detecting SF4 gas: a DFT NBO and QTAIM investigation, Appl. Surf. Sci. 510 (2020) 145490.
[35] M. Dagani, H. Barda, T. Benya, D. Sanders, Bromine Compounds in Ullmann's Encyclopedia of Industrial Chemistry, Wiley-VCH Publications, Weinheim, 2000.
[36] K.S. Patel, A.K. Patel, H.H. Chaudhary, D.J. Sen, Cease fire: an emergency practice in domestic as well as in profession, Res. J. Sci. Technol. 6 (2014) 133–142.
[37] J. Scaranto, S. Giorgianni, Insights into the adsorption of CH2BrF on anatase TiO2 (1 0 1) surface through DFT modelling, Comput. Mater. Sci. 81 (2014) 556–560.
[38] M.D. Esrafili, N2O reduction over a fullerene-like boron nitride nanocage: a DFT study, Phys. Lett. A 381 (2017) 2085–2091.
[39] R. Gholizadeh, Y.-X. Yu, N2O+ CO reaction over Si-and Se-doped graphenes: an ab initio DFT study, Appl. Surf. Sci. 357 (2015) 1187–1195.
[40] A.J. Hassan, Hydrochlorofluorocarbons adsorption on undoped and Al-doped graphene nanoflakes by using density functional theory (DFT) study, Russian J. Phys. Chem. B 13 (2019) 1064–1069.
[41] W. Yang, Z. Gao, X. Liu, C. Ma, X. Ding, W. Yan, Directly catalytic reduction of NO without NH3 by single atom iron catalyst: a DFT calculation, Fuel 243 (2019) 262–270.
[42] J. Scaranto, D. Moro, N. Tasinato, P. Stoppa, S. Giorgianni, Insights into the interaction between CH2F2 and titanium dioxide: DRIFT spectroscopy and DFT analysis of the adsorption energetics, Spectrochim. Acta Part A Mol. Biomol. Spectrosc. 136 (2015) 1614–1620.
[43] F. Zasada, P.V.B. Pinho, W. Piskorz, C. Hudy, J. Janas, J. Grybos, K. Góra-Marek, Z. Sojka, Adsorption of NO2 and NO3 on cobalt spinel nanocubes and interfacial dynamics of the resultant NOx adspecies (x= 1, 2, 3)–a DFT, atomistic thermodynamic, IR and isotopic exchange study, J. Phys. Chem. C (2020).
[44] J.P. Perdew, K. Burke, M. Ernzerhof, Generalized gradient approximation made simple, Phys. Rev. Lett. 77 (1996) 3865.
[45] S. Grimme, Accurate description of van der Waals complexes by density functional theory including empirical corrections, J. Comput. Chem. 25 (2004) 1463–1473.
[46] S. Grimme, J. Antony, S. Ehrlich, H. Krieg, A consistent and accurate ab initio parametrization of density functional dispersion correction (DFT-D) for the 94 elements H-Pu, J. Chem. Phys. 132 (2010) 154104.
[47] S. Grimme, S. Ehrlich, L. Goerigk, Effect of the damping function in dispersion corrected density functional theory, J. Comput. Chem. 32 (2011) 1456–1465.
[48] W.J. Hehre, R. Ditchfield, J.A. Pople, Self—consistent molecular orbital methods. XII. Further extensions of Gaussian—type basis sets for use in molecular orbital studies of organic molecules, J. Chem. Phys. 56 (1972) 2257–2261.
[49] M. Frisch, G. Trucks, H. Schlegel, G. Scuseria, M. Robb, J. Cheeseman, G. Scalmani, V. Barone, G. Petersson, H. Nakatsuji, Gaussian 16, Gaussian, Inc. Wallingford, CT, 2016.
[50] M.J. Frisch, G.W. Trucks, H.B. Schlegel, G.E. Scuseria, M.A. Robb, J.R. Cheeseman, G. Scalmani, V. Barone, G.A. Petersson, H. Nakatsuji, X. Li, M. Caricato, A.V. Marenich, J. Bloino, B.G. Janesko, R. Gomperts, B. Mennucci, H.P. Hratchian, J.V. Ortiz, A.F. Izmaylov, J.L. Sonnenberg, Williams, F. Ding, F. Lipparini, F. Egidi, J. Goings, B. Peng, A. Petrone, T. Henderson, D. Ranasinghe, V.G. Zakrzewski, J. Gao, N. Rega, G. Zheng, W. Liang, M. Hada, M. Ehara, K. Toyota, R. Fukuda, J. Hasegawa, M. Ishida, T. Nakajima, Y. Honda, O. Kitao, H. Nakai, T. Vreven, K. Throssell, J.A. Montgomery Jr., J.E. Peralta, F. Ogliaro, M.J. Bearpark, J.J. Heyd, E.N. Brothers, K.N. Kudin, V.N. Staroverov, T.A. Keith, R. Kobayashi, J. Normand, K. Raghavachari, A.P. Rendell, J.C. Burant, S.S. Iyengar, J. Tomasi, M. Cossi, J.M. Millam, M. Klene, C. Adamo, R. Cammi, J.W. Ochterski, R.L. Martin, K. Morokuma, O. Farkas, J.B. Foresman, D.J. Fox, Gaussian 16 Rev. C.01, Wallingford, CT, 2016.
[51] T. Lu, F. Chen, Multiwfn: a multifunctional wavefunction analyzer, J. Comput. Chem. 33 (2012) 580–592.
[52] N.M. O'boyle, A.L. Tenderholt, K.M. Langner, Cclib: a library for package-independent computational chemistry algorithms, J. Comput. Chem. 29 (2008) 839–845.
[53] R.G. Parr, R.A. Donnelly, M. Levy, W.E. Palke, Electronegativity: the density functional viewpoint, J. Chem. Phys. 68 (1978) 3801–3807.
[54] T. Koopmans, Über die Zuordnung von Wellenfunktionen und Eigenwerten zu den einzelnen Elektronen eines Atoms, Physica 1 (1934) 104–113.
[55] J. Janak, Proof that∂ e∂ n i= ε in density-functional theory, Phys. Rev. B 18 (1978) 7165.
[56] K.B. Wiberg, Application of the pople-santry-segal CNDO method to the cyclopropylcarbinyl and cyclobutyl cation and to bicyclobutane, Tetrahedron 24 (1968) 1083–1096.
[57] A.E. Reed, L.A. Curtiss, F. Weinhold, Intermolecular interactions from a natural bond orbital, donor-acceptor viewpoint, Chem. Rev. 88 (1988) 899–926.
[58] S. Grimme, Semiempirical GGA-type density functional constructed with a long-range dispersion correction, J. Comput. Chem. 27 (2006) 1787–1799.
[59] J.B. Foresman, A. Frisch, Exploring chemistry with electronic structure methods: a guide to using Gaussian, (1996).
[60] S.S. Li, Semiconductor Physical Electronics, Springer Science & Business Media, 2012.
[61] K.H. Hendriks, W. Li, M.M. Wienk, R.A. Janssen, Small-bandgap semiconducting polymers with high near-infrared photoresponse, J. Am. Chem. Soc. 136 (2014) 12130–12136.

[62] A.J. Foster, F. Weinhold, Natural hybrid orbitals, J. Am. Chem. Soc. 102 (1980) 7211–7218.
[63] C.F. Matta, Hydrogen–Hydrogen Bonding: The Non-Electrostatic Limit of Closed-Shell Interaction Between Two Hydro, Hydrogen Bonding—New Insights, Springer, 2006, pp. 337–375.
[64] H.J. Bohórquez, R.J. Boyd, C.F. Matta, Molecular model with quantum mechanical bonding information, J. Phys. Chem. A 115 (2011) 12991–12997.
[65] S.J. Grabowski, QTAIM characteristics of halogen bond and related interactions, J. Phys. Chem. A 116 (2012) 1838–1845.
[66] E.R. Johnson, S. Keinan, P. Mori-Sánchez, J. Contreras-García, A.J. Cohen, W. Yang, Revealing noncovalent interactions, J. Am. Chem. Soc. 132 (2010) 6498–6506.
[67] J. Contreras-García, E.R. Johnson, S. Keinan, R. Chaudret, J.-P. Piquemal, D. N. Beratan, W. Yang, NCIPLOT: a program for plotting noncovalent interaction regions, J. Chem. Theory Comput. 7 (2011) 625–632.